Nck enables directional cell migration through the coordination of polarized membrane protrusion with adhesion dynamics

Sankar P. Chaki[1], Rola Barhoumi[2], Matthew E. Berginski[3], Harini Sreenivasappa[4], Andreea Trache[4], Shawn M. Gomez[3] and Gonzalo M. Rivera[1,*]

[1]Department of Veterinary Pathobiology, Texas A&M University, College Station, TX 77843-4467, USA
[2]Department of Veterinary Integrative Biosciences, Texas A&M University, College Station, TX 77843-4467, USA
[3]Department of Biomedical Engineering, University of North Carolina, Chapel Hill, NC 27599-7575, USA
[4]Department of Systems Biology and Translational Medicine, Texas A&M University Health Science Center, College Station, TX 77843-1114, USA
*Author for correspondence (grivera@cvm.tamu.edu)

Accepted 21 January 2013
Journal of Cell Science 126, 1637–1649

doi: 10.1242/jcs.119610

Summary

Directional migration requires the coordination of cytoskeletal changes essential for cell polarization and adhesion turnover. Extracellular signals that alter tyrosine phosphorylation drive directional migration by inducing reorganization of the actin cytoskeleton. It is recognized that Nck is an important link between tyrosine phosphorylation and actin dynamics; however, the role of Nck in cytoskeletal remodeling during directional migration and the underlying molecular mechanisms remain largely undetermined. In this study, a combination of molecular genetics and quantitative live cell microscopy was used to show that Nck is essential in the establishment of front–back polarity and directional migration of endothelial cells. Time-lapse differential interference contrast and total internal reflection fluorescence microscopy showed that Nck couples the formation of polarized membrane protrusions with their stabilization through the assembly and maturation of cell–substratum adhesions. Measurements by atomic force microscopy showed that Nck also modulates integrin α5β1-fibronectin adhesion force and cell stiffness. Fluorescence resonance energy transfer imaging revealed that Nck depletion results in delocalized and increased activity of Cdc42 and Rac. By contrast, the activity of RhoA and myosin II phosphorylation were reduced by Nck knockdown. Thus, this study identifies Nck as a key coordinator of cytoskeletal changes that enable cell polarization and directional migration, which are crucial processes in development and disease.

Key words: Nck, Cell adhesion, Actin cytoskeleton, Cell polarity, Directional migration

Introduction

Reorganization of the cytoskeletal architecture is the driving force behind morphological and functional changes involved in persistent cell migration (Friedl and Wolf, 2010; Gardel et al., 2010; Petrie et al., 2009). Deciphering how cytoskeletal remodeling and signaling networks are spatially and temporally coordinated during directional, persistent cell migration remains a crucial challenge.

The cell migration cycle involves the establishment of a front–rear axis of polarity, successive cycles of membrane protrusion, adhesion to the substratum, forward propulsion of the cell body, and disengagement of the trailing edge (Lauffenburger and Horwitz, 1996). Extracellular signals that alter tyrosine phosphorylation, including growth factors and fibrils of the extracellular matrix, promote cytoskeletal rearrangements that coordinate the steps in the cell migration cycle (Casaletto and McClatchey, 2012; Geiger and Yamada, 2011; Huttenlocher and Horwitz, 2011). Signaling by tyrosine phosphorylation relies on recognition by proteins containing a Src homology (SH) 2 domain (Machida and Mayer, 2005; Pawson, 2004) such as the Nck adaptors. The Nck family of SH2/SH3 domain-containing adaptors, consisting of Nck1/α and Nck2/β (Buday et al., 2002; Li et al., 2001), is required during development (Bladt et al., 2003) and is involved in cytoskeletal remodeling underlying pathogen–host cell interactions (Campellone et al., 2004; Gruenheid et al., 2001; Moreau et al., 2000; Scaplehorn et al., 2002), T-cell receptor activation (Barda-Saad et al., 2005; Lettau et al., 2009), invadopodia formation (Oser et al., 2010; Stylli et al., 2009), cell adhesion and motility (Abella et al., 2010; Antoku et al., 2008; Guan et al., 2009; Lapetina et al., 2009; Rivera et al., 2006; Ruusala et al., 2008), and intercellular junction organization in kidney podocytes (Jones et al., 2006; Verma et al., 2006). Nck1 and Nck2 have broad and overlapping expression patterns and are believed to have mostly redundant functions (Bladt et al., 2003), however, non-compensating roles depending on the specific cellular and signaling context have also been suggested (Guan et al., 2007; Guan et al., 2009; Hu et al., 2009).

We and others demonstrated that Nck adaptors are involved in cytoskeletal rearrangements leading to the formation of dorsal membrane ruffles induced by growth-factors (Abella et al., 2010; Rivera et al., 2006; Ruusala et al., 2008). Previously, we showed that Nck promotes localized actin polymerization through the activation of the N-WASp/Arp2/3 pathway (Rivera et al., 2004) by a mechanism that involves cooperation with phosphoinositides (Rivera et al., 2009). The formation of protrusions at the edge of

migrating cells, on the other hand, is mediated by Arp2/3-dependent actin polymerization stimulated by the related WAVE proteins (Suetsugu et al., 2003). Although early studies linked Nck to the activation of the WAVE complex (Eden et al., 2002), recent investigations suggest that activation involves phosphorylation of complex components and simultaneous interactions with Rac-GTP and acidic phospholipids (Lebensohn and Kirschner, 2009). More recently, a role for a complex consisting of Nck and WAVE2 in the phagocytosis of human-restricted CEACAM-binding bacteria has been described (Pils et al., 2012). Thus, the role played by Nck-dependent actin remodeling in the formation of polarized protrusions in migrating cells remains undetermined.

Current models postulate a mechanical and biochemical coupling between actin dynamics and the assembly/disassembly of adhesion structures in migrating cells (Gardel et al., 2010). Although Nck adaptors are involved in cell adhesion and motility (Stoletov et al., 2001; Vaynberg et al., 2005), it is currently unknown if the assembly and turnover of adhesion structures is modulated by Nck. We hypothesized that the Nck family contributes to endothelial cell motility and morphogenesis by coordinating protrusion at the leading edge with adhesion turnover. Here we show that abrogation of Nck signaling in endothelial cells leads to deficient migration and impaired directionality due, primarily, to the loss of a front–rear axis of polarity, the formation of transient/unstable membrane protrusions, and disruption of adhesion turnover. Importantly, our live cell imaging studies reveal that modulation of the spatiotemporal activation of the Rho GTPases by Nck is a key molecular mechanism involved in endothelial cell morphodynamics.

Results

Nck regulates directional motility through modulation of protrusion dynamics

Although it is generally assumed that Nck1 and Nck2 have mostly overlapping functions, their individual contribution to cell motility has not been determined. The expression of both Nck1 and Nck2 in HUVEC was confirmed by semi-quantitative RT-PCR (supplementary material Fig. S1B). We used a loss-of-function approach based on the expression of short hairpin RNAs that consistently induced a ~90% and ~50% decrease of mRNA/protein levels of Nck1 or Nck2, respectively (supplementary material Fig. S1C–F). Rescue of double knockdown cells (simultaneous targeting of Nck1 and Nck2) with retroviral particles harboring a shRNA-resistant Nck2 cDNA resulted in expression levels ~2 fold above that of the endogenous Nck. Since commercially available Nck antibodies do not discriminate between Nck1 versus Nck2, we confirmed the specificity of the targeting shRNAs in Nck-deficient (inactivation of both Nck genes) mouse embryonic fibroblasts expressing fluorescently-labeled Nck1 (supplementary material Fig. S1C) or Nck2 (supplementary material Fig. S1E). We first tested the role of Nck adaptors in directional cell migration in two dimensions using a conventional wound-healing assay (Rodriguez et al., 2004). Compared with control cells, depletion of Nck1, Nck2 or both (Nck1 and Nck2) led to a well discernible impairment in directional migration 24 hours after the wounding of confluent monolayers (Fig. 1A). The effects of Nck1 versus Nck2 depletion were comparable and there was only a subtle additive effect when both adaptors were simultaneously targeted. The expression of shRNA-insensitive Nck2 in double knockdown cells induced significant ($P<0.05$) restoration of their migration capacity. Quantitative image analysis confirmed a significant ($P<0.001$) 40–60% decrease in directional migration induced by Nck depletion (Fig. 1B). Importantly, cell numbers and viability determined in parallel cultures did not differ ($P<0.05$) among experimental conditions (not shown). In addition, the double knockdown phenotype was rescued to the same extent by re-expression of either Nck isoform alone or in combination (supplementary material Fig. S2).

Productive cell migration involves the establishment of a front–rear axis of polarity, successive cycles of membrane protrusion, adhesion to the substratum, forward propulsion of the cell body, and disengagement of the trailing edge. Therefore, given the defects in two-dimensional migration observed in Nck-depleted cells, we asked what steps along the migration cycle are affected by perturbation of Nck signaling. Time-lapse DIC imaging was performed to analyze patterns of membrane protrusion in unstimulated and VEGF-stimulated HUVEC in subconfluent cultures (supplementary material Movie 1). Differential patterns of membrane activity in Nck-knockdown versus control and rescued cells could be readily appreciated by visual inspection of kymographs (Fig. 1C). Surprisingly, quantitative analysis revealed an increased ($P<0.001$) rate of protrusion and ruffle frequency, but decreased protrusion persistence, in Nck-depleted (simultaneous knockdown of Nck1 and Nck2) versus control or rescued cells under unstimulated (starvation) conditions (Fig. 1D). Similar trends determined for retraction velocity and persistence (data not shown) suggest that, at least under basal conditions, interference with Nck signaling leads to bursts of transient protrusions. On the other hand, VEGF stimulation elicited a significant ($P<0.001$) increase in protrusion velocity and ruffle frequency while decreasing protrusion persistence in control and rescued cells. In contrast, a decrease in protrusion velocity and ruffle frequency accompanied by a slight increase in protrusion persistence was observed in Nck-depleted cells in response to VEGF (Fig. 1D).

To further test the role of Nck in membrane protrusion dynamics, we analyzed kinetic parameters of nascent protrusions formed soon after ATP replenishment in cells briefly exposed to low concentration of sodium azide, a treatment known to block actin filament assembly by depleting the pool of ATP-loaded actin monomers (Bear et al., 2002; Bladt et al., 2003; Svitkina et al., 1986). Consistent with the findings under starvation, kymographs derived from DIC time-lapse imaging (see supplementary material Movies 2, 3) showed bursts of transient protrusive activity following ATP replenishment in cells with simultaneous knockdown of Nck 1 and Nck2, but not in control or Nck-rescued cells (supplementary material Fig. S3). Collectively, these results suggest that Nck adaptors modulate directional cell migration by a mechanism that limits unproductive, transient cycles of membrane protrusion and retraction. In addition, these observations provide indirect evidence that the activity of actin nucleators, such as the Arp2/3 complex, is not directly compromised by disruption of Nck-dependent signaling.

Nck plays an important role in the modulation of adhesion turnover

Current views support the presence of a mechanical and biochemical coupling between actin dynamics and the

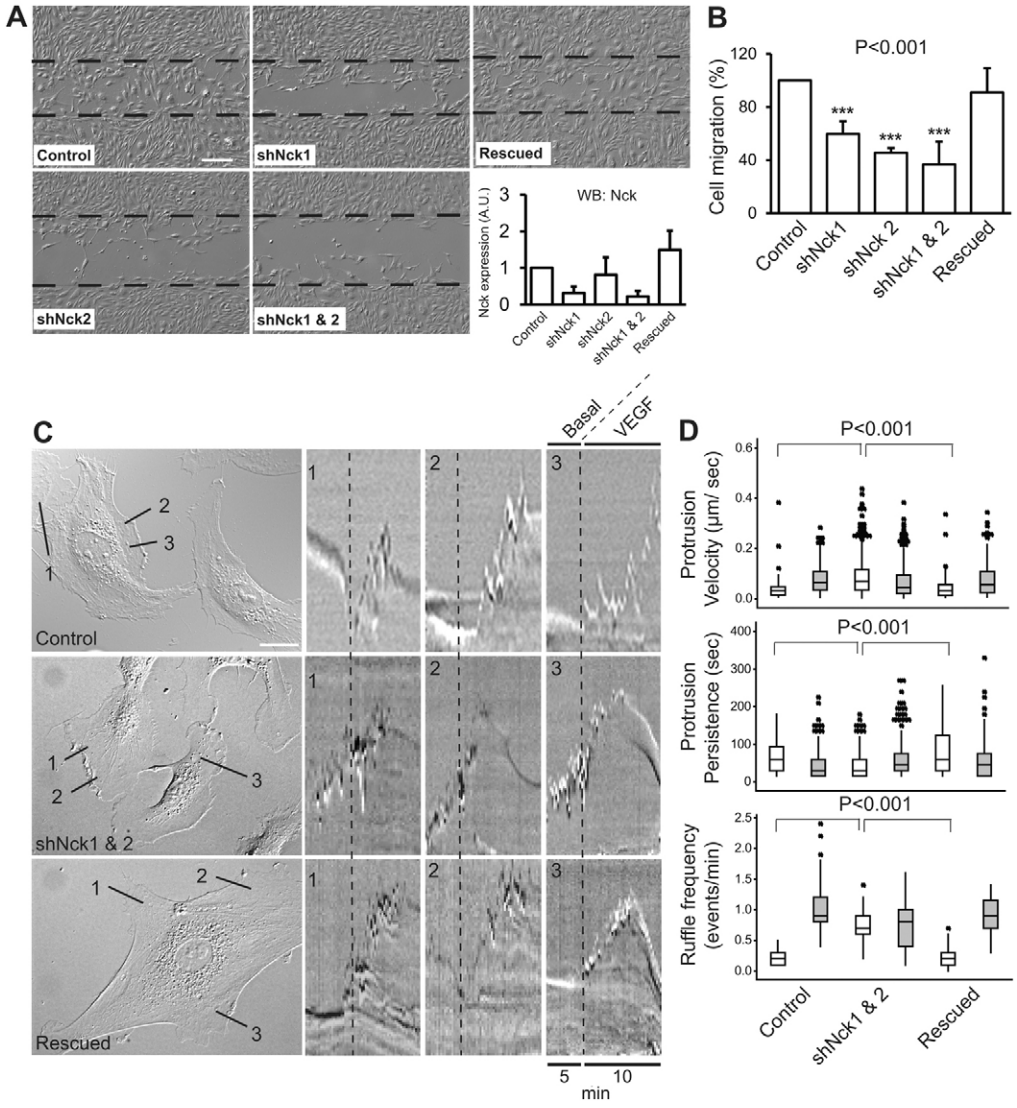

Fig. 1. Nck is required for two-dimensional migration and modulation of membrane protrusion dynamics. (**A**) DIC images of the same fields were taken at 0 and 24 hours after wounding confluent monolayers of serum-starved HUVEC plated on fibronectin-coated surfaces. The wound (dotted black lines) was allowed to repair in the presence of starvation medium supplemented with VEGF. Scale bar: 200 µm. The bar graph shows expression levels of Nck proteins relative to GAPDH level (mean ± s.d., $n=3$). (**B**) Cells migrating into the wound were counted, and results expressed as percentage of controls. Bars are mean ± s.d. ($n=3$ independent experiments); ***$P<0.001$ versus control. (**C**) Representative frames from time-lapse videos (left panels) and kymographs (three right panels) obtained from the same cell before and after VEGF stimulation. Subconfluent HUVEC monolayers were serum-starved for 2 hours before DIC images were collected at 15-second intervals for 5 minutes before (Basal) and 10 minutes after stimulation with VEGF. Multiple kymographs ($n=4$–6) were generated from each cell using the EMBL ImageJ software. (**D**) Quantitative analysis of protrusion activity. The analysis included a total of 9–12 cells per treatment from each experiment ($n=3$ independent experiments). Statistical differences across cell populations (control, shNck1 and 2, and rescued) within each treatment (starvation versus VEGF) are indicated. Differences between treatments (starvation, open boxes versus VEGF stimulation, grey boxes) within each cell population (control, shNck1 and 2, and rescued) also reached statistical significance ($P<0.001$).

assembly/disassembly of adhesion structures in migrating cells (Gardel et al., 2010). Our results suggest that actin polymer elongation and branching, indirectly assessed by membrane protrusion dynamics (Fig. 1; supplementary material Fig. S3; supplementary material Movies 1–3), are not compromised when Nck signaling is abrogated. Therefore, the migration defects observed in Nck-depleted cells (Fig. 1A,B; supplementary material Fig. S2) could be linked to altered adhesion dynamics. To begin to understand the role of Nck in the modulation of cell–substratum adhesion, we first analyzed the subcellular distribution of Nck in control endothelial cells coexpressing fluorescently labeled paxillin, a signaling protein associated with focal adhesions. High levels of colocalization of paxillin and Nck2 at focal adhesions were, indeed, revealed by TIRF imaging (Fig. 2A,B). Calculated Pearson's correlation coefficient of 0.54±0.06 (mean ± s.d.; $n=14$ cells) showed significant colocalization (Zinchuk and Zinchuk, 2008). We also predicted a high level of colocalization of the two Nck isoforms in adhesion structures. To test this prediction, we performed localization experiments in HUVEC coexpressing Nck1/YFP and Nck2/mCherry. TIRF microscopy showed a high level of colocalization of Nck isoforms in adhesion structures of various sizes (Fig. 2C).

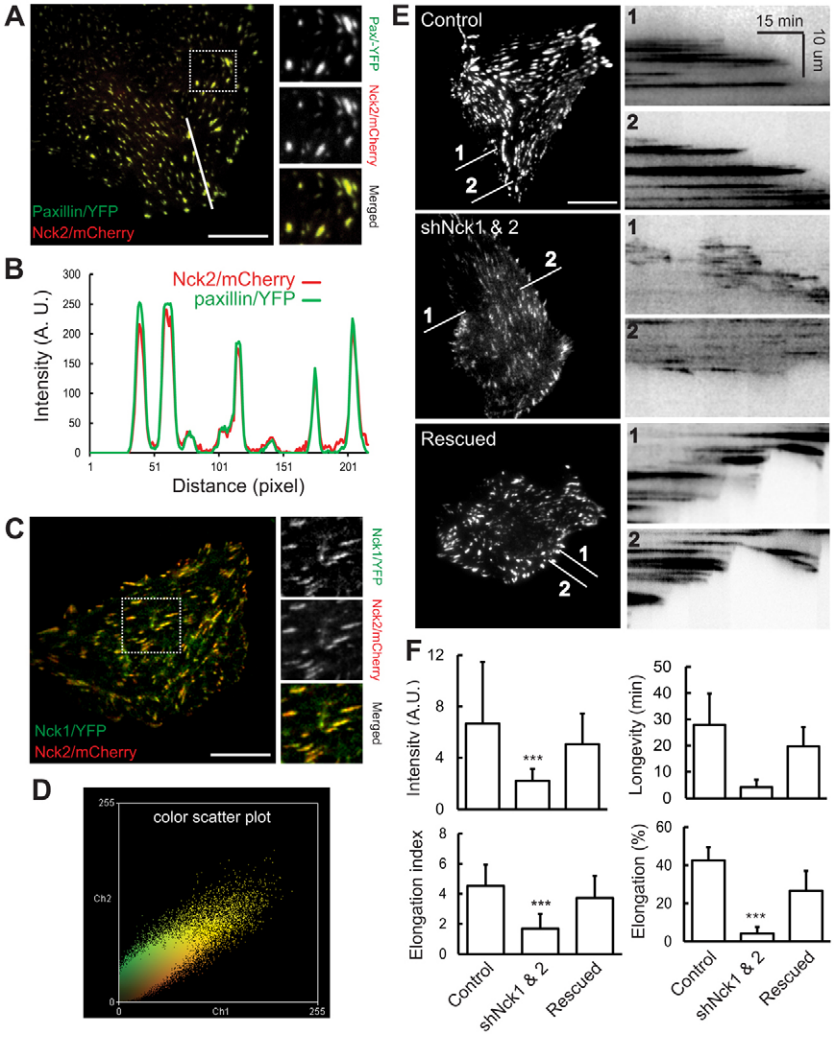

Fig. 2. Nck localizes to cell–matrix adhesion structures and regulates longevity of newly formed adhesions in protruding areas. (**A**) Representative TIRF images of HUVEC coexpressing Nck2/mCherry and paxillin/YFP. Boxed area is shown on the right at higher magnification. (**B**) Line-scans (corresponding to the white line shown in the merged image in A) showing a tight correlation of Nck/mCherry and Paxillin/YFP fluorescence intensity at adhesion sites. (**C**) Representative TIRF images of HUVEC coexpressing Nck2/mCherry and paxillin/YFP. (**D**) Color scatter plot corresponding to the image of the whole cell shown in C. Pearson's correlation coefficient of 0.68±0.103 (mean ± s.d., $n=11$ cells) shows a high level of colocalization of Nck1 and Nck2 isoforms. (**E**) Images extracted from time-lapse TIRF series obtained from cells expressing paxillin-YFP (left panels). Numbered white lines indicate protruding areas where kymographs were derived (right panels; two kymographs/cell are shown). Notice that adhesions located at the cell periphery are smaller and/or dimmer in Nck-depleted versus control or rescued cells. (**F**) Spatially restricted analysis, based on kymographs extracted from protruding areas, showing decreased intensity and longevity of peripheral adhesions in Nck knockdown cells. The elongation index and percentage of maturing adhesions were also calculated for new adhesions forming in protruding areas. ***$P<0.001$ versus corresponding control. Scale bars: 20 µm.

High colocalization is readily apparent from both fluorescence overlay images (Fig. 2C) and color scatter plots (Fig. 2D), which are in agreement with a Pearson's correlation coefficient of 0.68±0.103 (mean ± s.d., $n=11$ cells).

To determine the role of Nck adaptors in the modulation of adhesion dynamics, we performed time-lapse TIRF imaging of control, Nck-deficient, and rescued cells expressing fluorescently-labeled paxillin. Visual inspection of the time-lapse series suggested that control and rescued cells formed nascent adhesions (Choi et al., 2008) in protruding areas that underwent maturation into focal complexes/focal adhesions (supplementary material Movies 4, 6). Interestingly, although occasional changes in directionality were observed due to the absence of guidance clues, these cells developed a front–rear axis of polarity characterized by the formation of major protrusion. Nck-depleted cells also formed nascent adhesions in protruding areas (cell periphery), but in contrast to control or rescued cells, these adhesion structures seemed to fail to mature into focal complexes/focal adhesions and appeared to undergo an accelerated turnover (supplementary material Movie 5). Since TIRF movies clearly suggested major differences in control/rescued versus Nck-depleted cells in the dynamics of peripheral adhesions, i.e. newly formed adhesions in the protruding areas, we first performed spatially restricted analysis of adhesion dynamics using previously described methods (Choi et al., 2008; Webb et al., 2004). Indeed, this analysis demonstrated that both the intensity and longevity of adhesions developing in protruding areas was significantly reduced ($P<0.001$) in Nck-depleted versus control or rescued cells (Fig. 2E,F). In addition, the elongation index (ratio between the long axis and the perpendicular axis) of maturing adhesions and the percentage of adhesions undergoing elongation was significantly decreased ($P<0.001$) in Nck-depleted cells compared to control/rescued cells (Fig. 2F).

These above results prompted us to assess whether Nck signaling affected cell–substratum adhesions at a global scale. To this aim, we used a recently developed analysis system for the automated detection, tracking, and quantification of adhesion structures in living cells (Berginski et al., 2011). This is a unique tool that allows the assessment of adhesion dynamics in a comprehensive, unbiased manner. Consistent with the findings of the spatially-restricted analysis, inspection of time-lapse series (Fig. 3A) and the quantitative analysis of adhesion dynamics at a global scale (Fig. 3B) show that adhesion structures in cells with Nck depletion have decreased ($P<0.001$) adhesion area, intensity, assembly/disassembly rates, and longevity when compared with control cells. In addition, the disassembly rate was significantly higher ($P<0.001$) in control than Nck-depleted

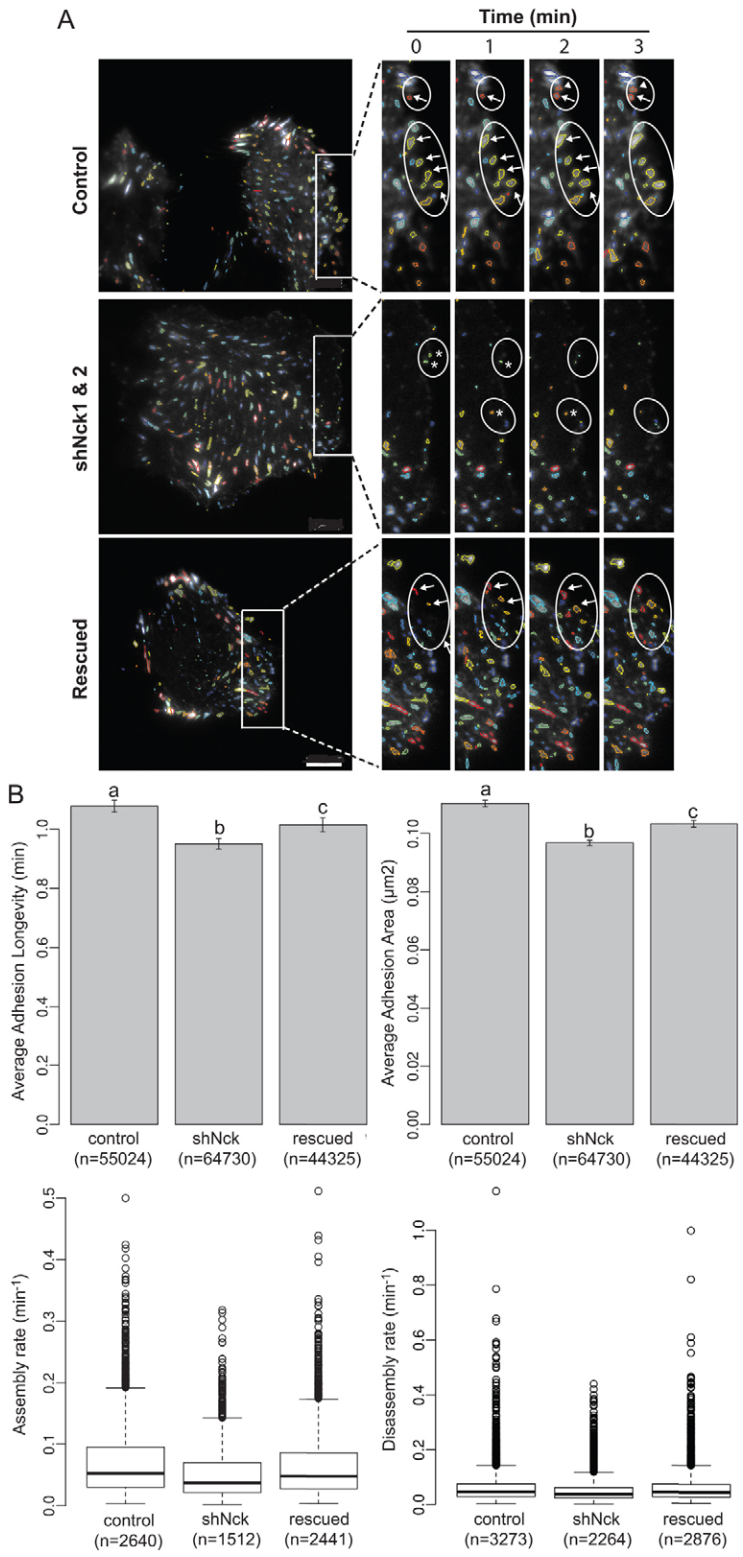

Fig. 3. Nck depletion alters adhesion turnover. TIRF imaging of HUVEC expressing paxillin-YFP was performed to monitor focal adhesion (FA) dynamics following ATP depletion and replenishment. High-resolution quantification of spatiotemporal dynamics of FA was performed using an analysis system for the automated detection, tracking and data extraction of these structures in living cells (see Materials and Methods). (**A**) Images of cells (left panels) and regions of interest (right panels) from selected frames extracted from time-lapse series following the processing with the tracking algorithm. The software assigns the same color to particular adhesion structures that are unambiguously detected in successive frames. Circled arrows and asterisks highlight persistent and transient adhesion structures, respectively. (**B**) Quantitative analysis showing parameters of adhesion dynamics in control, Nck-depleted (shNck) and rescued cells. The analysis included a total of 10–13 time-lapse series (cells) from each treatment. Bars (mean, with 95% confidence intervals, top panels) with different letters are significantly different ($P<0.0001$). The box plots (bottom panels) summarize the data of assembly and disassembly rates for adhesions with curve fits for paxillin intensity.

cells or rescued cells. It remains unclear why re-expression of Nck2 failed to fully rescue the disassembly rate of adhesion structures. Nevertheless, the comprehensive analysis of adhesion dynamics reveals that Nck depletion is linked to altered patterns of adhesion turnover. Remarkably, the formation of smaller, short-lived adhesion structures at the cell periphery is consistent with the formation of transient and non-polarized protrusion events in response to abrogation of Nck signaling. Collectively, our studies of cell migration and colocalization suggest important functional redundancy between Nck1 and Nck2.

Integrin α5β1-fibronectin adhesion force and cell stiffness are modulated by Nck

The findings that Nck signaling affects the longevity, size/intensity, and assembly/disassembly rates of adhesions at a global scale prompted us to probe the role of this pathway in structural, mechanical, and functional properties of the cytoskeleton using atomic force microscopy (AFM). Endothelial cells express $\alpha5\beta_1$ integrins (Paik et al., 2001) which are known to be the specific adhesion receptor for fibronectin (Humphries et al., 2006). Using an AFM probe functionalized with fibronectin (Trache et al., 2005), integrin-dependent adhesion forces and cell stiffness were compared in cells with normal or altered Nck signaling. As shown in Fig. 4A, both the adhesion force and cell stiffness were significantly decreased ($P<0.05$) in Nck-depleted compared to control or rescued cells. Consistent with these observations, the morphology of the actin cytoskeleton showed important qualitative differences (Fig. 4B); (i) a single, polarized protrusion was evident in the majority of control and rescued cells whereas most of the Nck-depleted cells presented numerous protrusions oriented in multiple directions, and (ii) prominent, well organized actin fibers were present in control and rescued cells but not in Nck-depleted cells. Quantitative analysis (Lim et al., 2010) showed that the F-actin area relative to cell area was reduced in cells with disruption of Nck signaling (Fig. 4C). Furthermore, the probability of integrin α5β1adhesion to fibronectin was significantly decreased in cells with Nck depletion versus control or rescued cells (Fig. 4A). Mechanistically, the decrease in adhesion force and cell stiffness observed in Nck-depleted cells was linked to a significant decrease ($P<0.05$) in the phosphorylation levels of serine 19 of myosin II regulatory light chain (Fig. 4D), a major phosphorylation site involved in the activation of myosin II by its primary kinases, including Rho-associated coiled coil-containing kinase (ROCK) (Vicente-Manzanares et al., 2009). Taken together, these results demonstrate that Nck-stimulated actin remodeling modulates α5β1 integrin-fibronectin adhesion force and cytoskeletal tension through phosphorylation-dependent activation of myosin II by a mechanism that involves the RhoA/ROCK pathway.

Perturbation of Nck signaling inhibits the establishment of a front-rear axis of cell polarity and directional migration

During the course of experiments designed to quantify protrusive activity (DIC imaging for 10–15 minutes), control and rescued, but not Nck knockdown cells, underwent an incipient polarization. To test whether Nck plays a role in the establishment of front–rear axis of polarity in crawling cells, we performed time-lapse DIC imaging for prolonged periods of time (up to 1 hour) of cells previously subjected to ATP depletion/replenishment as described above. The application of a uniform motogenic signal (ATP replenishment) activates the basic motility machinery, and in the absence of a chemotactic signal or other directional clue, this assay enables the assessment of mechanisms of intrinsic cell directionality (Petrie et al., 2009).

A

	Force (pN)		Stiffness (kPa)		Adhesion probability (%)	Number of individual measurements
	estimated peak value	95% C.I.	estimated peak value	95% C.I.		
Control	41	40.2 – 41.8	20	19.4 – 20.7	40	1,924
shNck1 & 2	30	29.6 – 30.4	8	8.1 – 8.3	26	1,905
Rescued	47	45.7 – 47.7	26	25.3 – 26.9	65	1,999

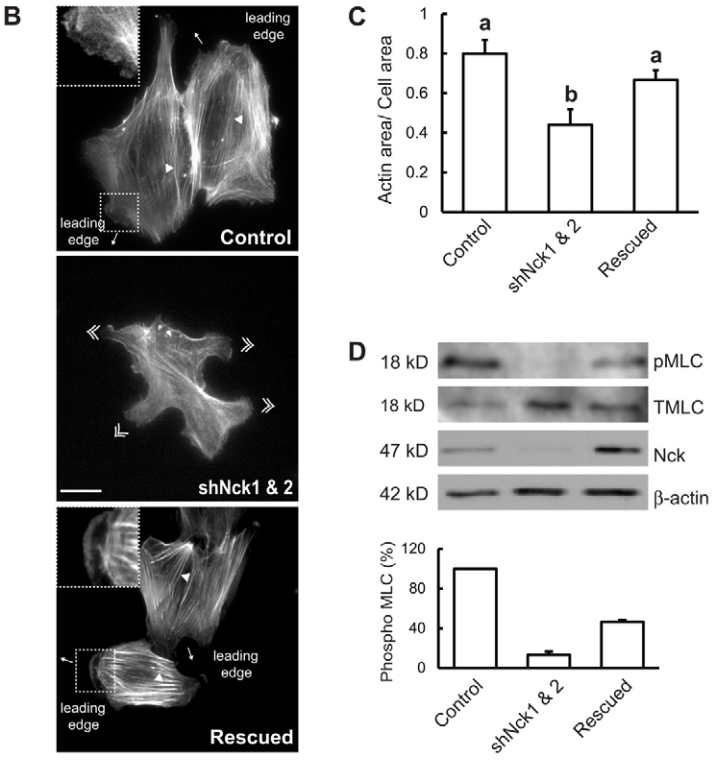

Fig. 4. Nck modulates cell adhesion strength to the matrix and cytoskeletal tension. (**A**) The cell adhesion and cytoskeletal properties of control, Nck-depleted (shNck) and rescued cells were probed using AFM. Estimated peak values and 95% confidence intervals (C.I.) are shown for the α5β1 integrin–fibronectin adhesion force and cell stiffness distributions. Kernel density plots of the distribution of force or elasticity values (number of individual measurements per treatment are shown in the last column) were generated using normal reference bandwidths and Gaussian kernel functions (Silverman, 1986). For comparisons, peaks whose confidence intervals did not overlap were considered significantly different ($P<0.05$) (see Materials and Methods). Probability of adhesion for each treatment is also included. (**B**) Representative confocal images of cells stained with fluorescent phalloidin showing the morphology of F-actin. Notice the presence of prominent stress fibers in control and rescued but not Nck-depleted cells. In most instances, the leading edge was readily identified in control and rescued cells. Instead, multiple protrusions were more frequently observed in Nck-depleted cells (double arrowheads). Scale bar: 20 μm. (**C**) F-actin/cell surface ratio for control, Nck-depleted (shNck1 and 2) and rescued cells. Bars represent the mean ± s.d. Different letters indicate statistical significance ($P<0.01$). (**D**) Representative western blots (top panel) showing phosphorylation (Ser19) of the regulatory light chain of myosin II (pMLC), total regulatory light chain (TMLC), Nck and β-actin (loading control). The intensity of bands was measured by densitometry and the ratios of pMLC to TMLC were normalized by β-actin and expressed as a percentage of control (bottom panel).

Control cells and Nck-depleted cells rescued with Nck2 (rescued) began to develop a front–rear axis of polarity within 15 minutes of ATP replenishment and, in spite of occasional changes in the direction of movement, maintained a distinct polarized morphology with readily recognizable leading and trailing edges (Fig. 5A; supplementary material Movies 2, 3). Unexpectedly, Nck-depleted cells (depletion of both Nck1 and Nck2) frequently adopted a spread or fragmented morphology characterized by the lack of a defined front–rear axis of polarity (Fig. 5A; supplementary material Movies 2, 3). Compared to control or rescued cells, Nck-depleted cells changed directionality (Fig. 5B, left panel, $P<0.05$) and formed simultaneous protrusions in multiple directions with higher frequency (Fig. 5B, right panel, $P<0.05$). In addition, protrusions occupied a larger proportion of the total cell perimeter in Nck-deficient cells versus control or rescued cells (Fig. 5B, middle panel, $P<0.05$).

To further test the role of Nck in the establishment of the front–rear axis of polarity, we estimated an index of polarity based on the orientation of the Golgi complex (Etienne-Manneville and Hall, 2001) in endothelial cells located at the edge of wounds traced in confluent monolayers. In polarized cells migrating in two dimensions after the wounding of confluent monolayers (Uetrecht and Bear, 2009), the Golgi complex is usually positioned between the leading edge and the nucleus. As shown in Fig. 5C, almost 80% of control cells and a slightly smaller percentage of rescued cells were clearly polarized. In contrast, only 40% ($P<0.05$ versus control) of Nck-depleted cells show a polarized orientation of the Golgi complex.

Based on our findings that Nck depletions causes an overall defect in cell migration (Fig. 1A,B) and in the establishment of the front–rear axis of polarity (Fig. 5), we hypothesized that Nck plays a significant role in directionality of migration. To test this hypothesis, we performed time-lapse DIC imaging of HUVEC induced to migrate following the wounding of confluent monolayers. From visual inspection of representative DIC time-lapse series (supplementary material Movie 7) and tracks of cell movement shown in Fig. 6A, it is readily apparent – at the population level – that control and rescued, but not Nck-depleted cells, migrated faster, over longer distances, and followed straighter paths. We also performed detailed quantitative analysis of migration patterns of representative cells from each population using commercially available software (Ibidi®) for the visualization and analysis of cell migration data. Migration trajectories were tracked for individual cells during a period of 12 hours. As shown in Fig. 6B and supplementary material Movie 8, migration paths of control and rescued cells were longer and less convoluted than those of Nck-depleted cells. Circular plots in Fig. 6C, representing the distribution of migrating cells at discrete angle intervals, show that Nck-depleted cells had significantly more scattered ($P<0.01$) trajectories than control or rescued cells. Similarly, the velocity (total path length/time), straightness (displacement/total path length) and forward migration index (Wu et al., 2012) were significantly decreased

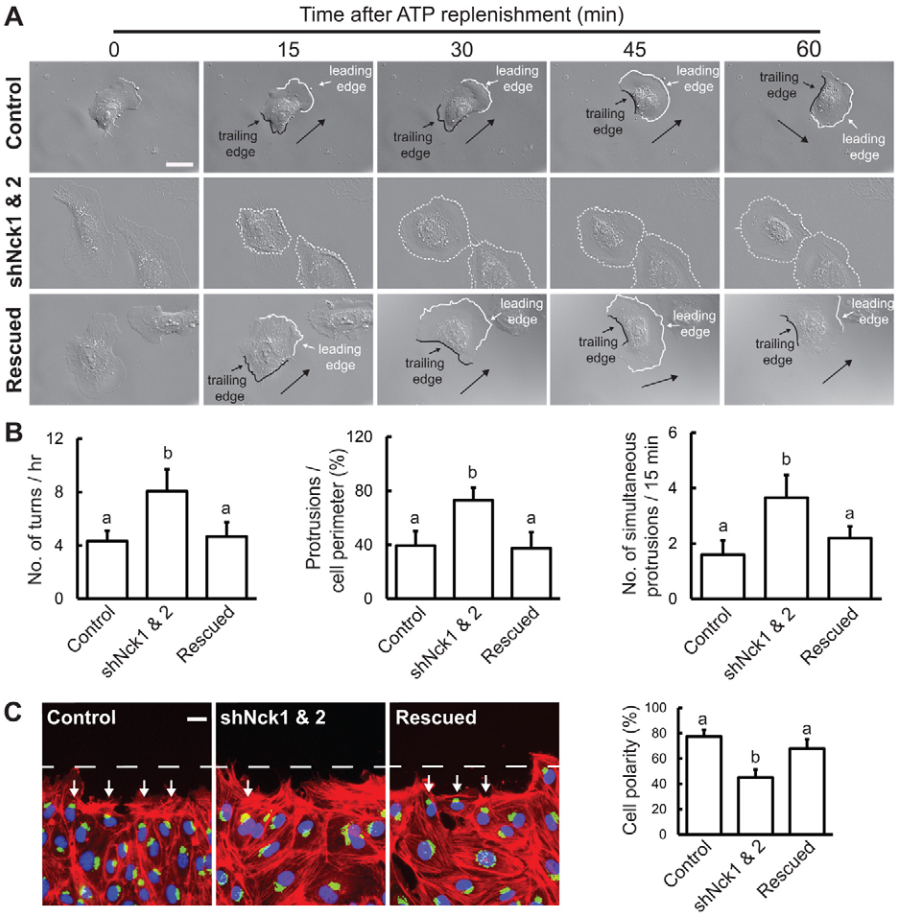

Fig. 5. Disruption of Nck signaling leads to loss of cell polarity. (**A**) Sub-confluent cultures of HUVEC were incubated with sodium azide for 30 minutes to induce ATP depletion. Following sodium azide washout, glucose-containing culture medium was replaced. Time-lapse DIC images were collected at 15-second intervals for 60 minutes following ATP replenishment. Continuous white and black traces highlight the leading and trailing edges (polarized cells), respectively, whereas the dotted white lines demark the borders of non-polarized cells. Black arrows indicate directionality of movement. Scale bar: 20 µm. (**B**) Quantitative analysis of cell polarity showing number (mean ± s.d.) of changes in directionality (turns, left panel); percentage of the total cell perimeter occupied by protrusions (middle panel) and number of simultaneously forming protrusions per 15-minute intervals (right panel). (**C**) Representative confocal images (left panel) of cells localized at the edge of a wound traced in confluent monolayers of HUVEC. Two hours after wounding the monolayers, cells were fixed and stained with an antibody against GM130 (Golgi marker), DAPI and Texas-Red phalloidin to visualize nuclei and F-actin, respectively. In polarized, migrating cells the Golgi complex is positioned between the cell's leading edge and the nucleus within an angle (120°) facing the major axis of the wound (white dotted line). White arrows indicate polarized cells. Scale bar: 25 µm. The percentage of polarized control, shNck 1 and 2, and rescued cells (mean ± s.d., right panel) was calculated by counting ~120 cell per treatment ($n=3$ independent experiments). Different letters indicate statistical significance ($P<0.01$).

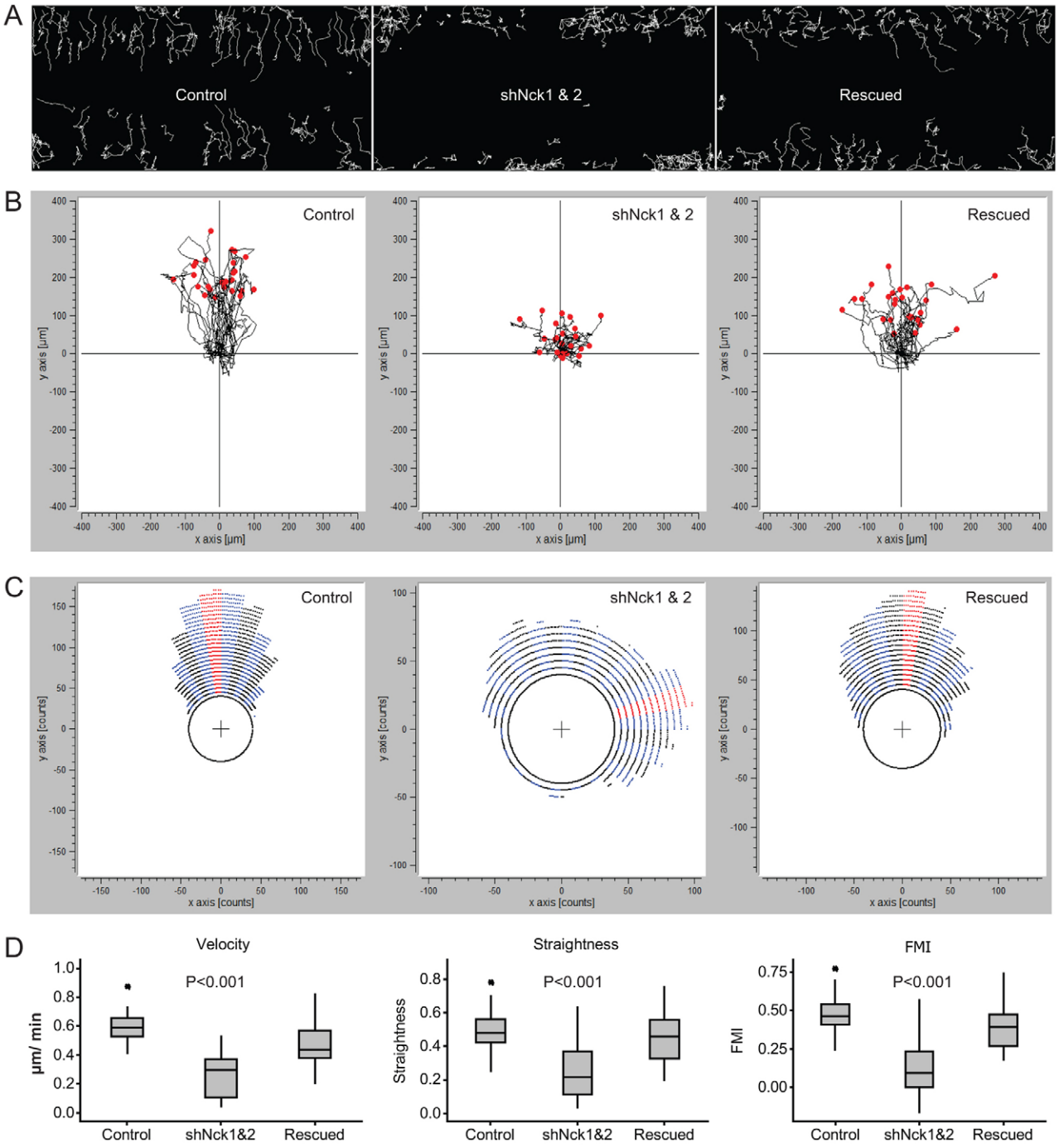

Fig. 6. Nck adaptors enable directional cell migration. Low magnification (5× objective) DIC time-lapse series were obtained (images collected at 15-minute intervals for 12 hours) and subsequently processed using cell-tracking algorithms. (**A**) Tracks of cells migrating in a representative field of imaging. (**B**) Detailed migration trajectories of representative cells ($n=26$) from control, Nck-depleted and rescued cells. Individual tracks were transposed so that each had its start at the origin. (**C**) Circular plots showing the distribution of the trajectories of migrating cells at discrete angle intervals. (**D**) Comparison of velocity (displacement/time), straightness (displacement/total path length) and forward migration index (FMI), defined as $\cos\theta=b/h$, where b is the y coordinate of the pair $y_i;x_i$ (the cell's end point of migration) and h is the net displacement of the cell measured by the straight line from the origin to the cell's end point of migration. $P<0.001$ for Nck-depleted cells compared with controls.

($P<0.001$) in cells with abrogation of Nck signaling but not control/rescued cells (Fig. 6D). Collectively, these results strongly suggest that Nck adaptors play an important role in directional cell migration through a mechanism that involves the specification of the front–rear axis of polarity.

Nck plays a crucial role in the coordination of the spatiotemporal activation of the Rho GTPases

The Rho GTPases Cdc42, Rac, and RhoA are molecular switches that play a key role in the regulation of the cytoskeleton and contribute to tissue morphogenesis by modulating intercellular

and cell–matrix adhesions, cell polarity, and membrane transport (Etienne-Manneville and Hall, 2002; Ridley, 2012). The activation of these master regulators of the cytoskeleton is governed by the abundance, subcellular distribution, and balance in the activity of guanine nucleotide exchange factors (GEFs), GTPase activating proteins (GAPs), and GDP-dissociation inhibitors (GDIs). It has been shown that the activation of RhoA at the cell's leading edge coincides with edge advancement and slightly precedes the subsequent local activation of Cdc42 and Rac (Machacek et al., 2009). Since abrogation of Nck signaling altered protrusion dynamics, adhesion turnover, and cell polarity, we hypothesized that Nck-dependent cytoskeletal changes are mediated by the Rho GTPases. To directly assess the role of Nck on the spatiotemporal activation of Rho GTPases we used the Raichu fluorescence resonance energy transfer (FRET)-based biosensors that monitor the activity balance between guanine nucleotide exchange factors (GEFs) and GTPase-activating proteins (GAPs) (Aoki and Matsuda, 2009). Our quantitative imaging experiments showed that activation of all three Rho GTPases was highly localized at the leading edge of crawling control and rescued cells (Fig. 7A; supplementary material Movies 9–11). Consistent with the formation of transient, multidirectional protrusions associated with short-lived cell–matrix adhesions, the activation of Cdc42 and Rac was significantly increased ($P<0.05$) and delocalized (unpolarized) in cells with depletion of Nck. RhoA activation in Nck knockdown cells was also delocalized, but in contrast to control and rescued cells, the overall levels of RhoA activation were reduced ($P<0.05$) by at least 50% (Fig. 7B; supplementary material Movies 9–11). Importantly, the impaired RhoA activation induced by abrogation of Nck signaling is consistent with decreased phosphorylation (activation) of myosin II regulatory light chain, reduced cell stiffness, limited incorporation of F-actin into stress fibers, and lack of maturation of cell–matrix adhesions forming in association with transient protrusions. Taken together these results strongly suggest that cytoskeletal changes induced by Nck are mediated by the Rho GTPases through a mechanism that involves regulation of the subcellular distribution and/or activity balance of a particular subset of GEFs and GAPs.

Discussion

Using a combination of molecular genetics and quantitative live-cell imaging we have uncovered an important role for Nck adaptors in directional cell migration that involves modulation of membrane protrusion dynamics, cell polarity, cytoskeletal tension and cell–matrix adhesion turnover. This study unveils new mechanistic insights whereby Nck integrates signaling by tyrosine phosphorylation with precise spatiotemporal activation of the Rho GTPases in the coordination of cytoskeletal dynamics. Of significance, our results point to Nck adaptors as critical players in endothelial cell morphogenesis and, therefore, relevant therapeutic targets in diseases associated with aberrant angiogenesis.

We (Ditlev et al., 2012; Rivera et al., 2006; Rivera et al., 2004; Rivera et al., 2009) and others (Bladt et al., 2003; Dodding and Way, 2009; Gruenheid et al., 2001; Jones et al., 2006; Scaplehorn et al., 2002) have demonstrated that Nck is a key regulator of

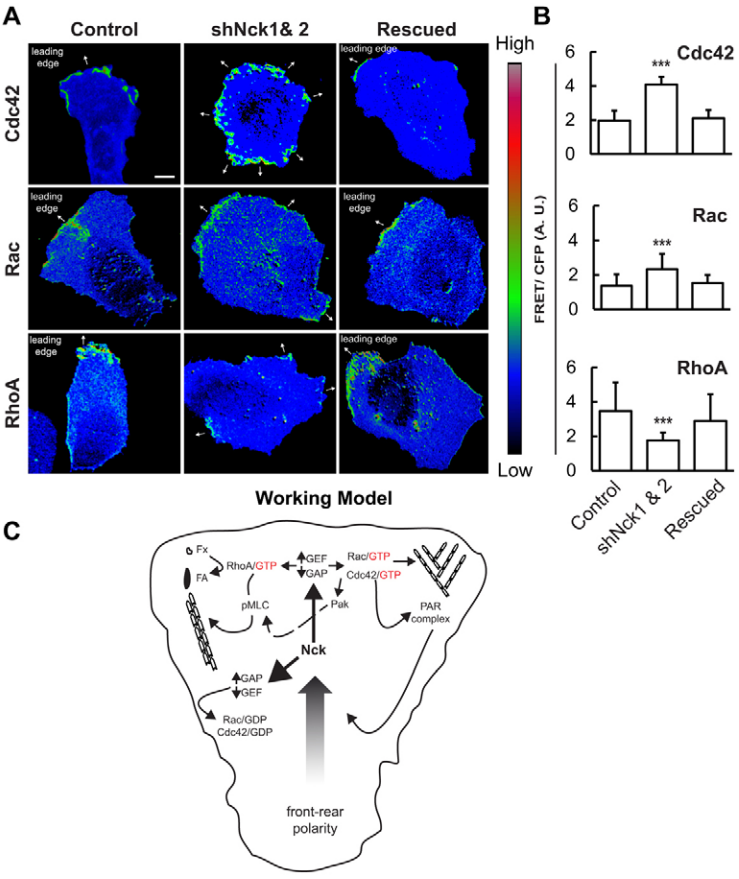

Fig. 7. Spatiotemporal activation of the Rho GTPases is altered in cells with aberrant Nck signaling. (**A**) Representative FRET/CFP ratio images extracted from time-lapse series obtained in control, shNck 1 and 2, or rescued cells expressing the FRET-based Raichu biosensors for Cdc42 (top row), Rac (middle row) and RhoA (bottom row). Scale bar: 10 µm. The FRET images are represented in the intensity modulated display. This mode associates color hue and the intensity of each hue with the image brightness; thus color represents activity. Red means high and blue low activity. The leading edge of polarized cells (control and rescued) is indicated by a single outward white arrow; multiple white arrows in non-polarized cells (shNck 1 and 2) point to multiple protruding areas. (**B**) Quantitative analysis of FRET activity based on 6–8 cells/treatment (mean ± s.d., $n=3$ independent experiments, ***$P<0.001$ versus control). (**C**) Role of Nck in the coordination of cytoskeletal changes involved in endothelial cell morphodynamics: a working model. Our data suggest that Nck regulates the subcellular localization and/or activity balance of a subset of GEF/GAPs. As a result, a net increase in the activity of GEFs at discrete sites on the plasma membrane leads to a 'symmetry break' and the controlled, localized activation of the Rho GTPases. Rac-dependent stimulation of localized actin polymerization leads to the formation of a major protrusion (leading edge). Nck may contribute indirectly, through the localized activation of Cdc42, to the stimulation of polarity pathways and the specification of the front–rear axis of polarity. Robust activation of RhoA at the cell's leading edge stimulates the formation of prominent stress fibers and ROCK-dependent phosphorylation of the regulatory light chain of myosin II (MLC). Increased actomyosin contractility, in turn, promotes the maturation of nascent adhesion/focal complexes (Fx) into focal adhesions (FA) that enable protrusion persistence and directional migration.

actin cytoskeletal dynamics. Here we used a number of complementary approaches to show that Nck-dependent cytoskeletal remodeling contributes to endothelial cell morphodynamics. The initiation of sprouting angiogenesis by endothelial cells relies on the acquisition of a mesenchymal phenotype characterized by the loss of cell–cell junctions, and the development of a migratory properties (Adams and Alitalo, 2007). Quite unexpectedly, our study shows that Nck promotes polarization of migrating endothelial cells by restricting transient lateral protrusions while enhancing the stability of a major leading edge protrusion by enabling adhesion maturation. Consistent with these findings control and rescued, but not Nck-depleted cells, migrated faster while maintaining directionality.

Accumulating evidence suggests a role for Nck in the orchestration of polarized cellular activities including localized actin polymerization at the site of T-cell receptor activation (Barda-Saad et al., 2005), the formation of invadopodia and associated matrix degradation in tumor cells (Oser et al., 2010; Oser et al., 2009; Stylli et al., 2009), the actin-dependent transport of Fas ligand to the immunological synapse (Lettau et al., 2006), and the organization of phagocytic cups stimulated by the cooperation between Nck and Cdc42 (Dart et al., 2012). We have previously shown that Nck interacts with p130Cas in growth factor-stimulated actin remodeling (Rivera et al., 2006) and recent findings suggests that Nck mediates p130Cas-dependent regulation of cell polarization through a pathway that involves Cdc42 activation (Funasaka et al., 2010). Results from our quantitative live-cell imaging experiments show that the loss of cell polarity in endothelial cells with Nck depletion is linked to dysregulation of the spatiotemporal activation of Cdc42, a master regulator of cell polarity (Nelson, 2009). Based on these findings we hypothesize that Nck regulates polarity pathways during vascular morphogenesis.

A number of vascular endothelial cell functions are regulated by activation of VEGF receptor 2 (VEGFR-2/Flk-1). Previous studies have involved Nck in VEGF-dependent activation of p21 GTPase-activated kinase Pak and regulation of endothelial cell migration (Lamalice et al., 2006; Stoletov et al., 2004; Stoletov et al., 2001). The second SH3 domain of Nck mediates the association with Pak (Galisteo et al., 1996), and this interaction is important for the localization of Pak to the plasma membrane (Lu et al., 1997). Pak, an important cytoskeletal effector downstream of the small GTPases Rac and Cdc42 (Bokoch, 2003), regulates cell migration by coupling leading-edge actin dynamics and focal adhesion turnover (Delorme-Walker et al., 2011). Our dynamic imaging studies disclose that, in addition to the loss of a front–rear axis of polarity, the unproductive migration of Nck-deficient cells is due to critical deficiencies in the coordination of cytoskeletal mechanics including i) the formation of unstable, multidirectional protrusions, ii) altered cell–matrix adhesion turnover including impaired maturation of protrusion-associated adhesions, iii) reduced integrin α5β1-fibronectin adhesion force and iv) decreased formation of F-actin into stress fibers and reduced cell stiffness. Consistent with these findings, Nck-depletion was associated with an altered pattern of spatiotemporal activation of the Rho GTPases characterized by increased, delocalized activation of Cdc42 and Rac and suppression of RhoA activation. Inhibition or depletion of Pak induces displacement of myosin IIA from the cell edge and a decrease in adhesion maturation (Delorme-Walker et al., 2011). Given that the complex Nck-Pak-Pix-PKL is recruited to focal adhesions (Brown et al., 2005), we hypothesize that Nck coordinates the recruitment of Pak to nascent adhesions and focal complexes in protruding areas, its activation by Cdc42/Rac, and the subsequent maturation of cell–matrix adhesions through combinatorial signaling from Pak- and RhoA-dependent pathways that regulate the localization and activation of myosin II.

RhoA-induced cytoskeletal tension correlates positively with stress fiber formation, integrin activation, and myosin II phosphorylation (Lim et al., 2012). That the abrogation of Nck signaling leads to a substantive decrease in myosin II phosphorylation constitutes a novel mechanistic insight provided by this study. Considerable work demonstrates that, by virtue of its actin filament cross-linking and contractile activities, myosin II plays an essential role in cell adhesion and migration (Vicente-Manzanares et al., 2009). Importantly, accumulating evidence suggests that myosin II contractility mediates the establishment of polarity in migrating cells through a mechanism whereby the local depletion/dislodging of the Rho guanine nucleotide exchange factor β-Pix (and others) decreases Rac activation, limits protrusiveness, and promotes RhoA-dependent adhesion maturation (Kuo et al., 2011; Vicente-Manzanares et al., 2011). In line with these observations, our results suggest that the Nck deficiency phenocopies – to a significant extent – the inactivation/depletion of myosin II which is characterized by increased protrusiveness, reduced adhesion maturation, and loss of cell polarity (Vicente-Manzanares et al., 2011; Vicente-Manzanares et al., 2007).

The FRET Raichu probes (Aoki and Matsuda, 2009) used in our study monitor the activity balance between GEFs and GAPs. We hypothesize that several aspects of the phenotype induced by Nck depletion result from an altered subcellular distribution and/or activity balance between critical GEFs and GAPs controlling the Rho GTPases. Consistent with this hypothesis, a recent study shows that the formation of unstable protrusions is linked to impaired directional motility in cells with SH3BP1 deficiency, a GAP that restricts Rac activation at the leading edge (Parrini et al., 2011). The present study lays the foundation for future work aimed at identifying which specific GEFs/GAPs are modulated by Nck adaptors and the elucidation of underlying molecular mechanisms.

In sum, these results highlight a central role for Nck in regulating critical aspects of cytoskeletal dynamics that drive vascular morphogenesis. Our findings lend support to a working model (Fig. 7C) underscoring Nck as a central node orchestrating the spatiotemporal activation of the Rho GTPases that, in turn, is required for the coordination of protrusion dynamics, adhesion turnover, and the establishment of a front–rear axis of polarity.

Materials and Methods

Reagents

Human umbilical vein endothelial cells (HUVEC), EBM2/EGM2 culture medium, HBSS, Trypsin-EDTA and TNS were purchased from Lonza (Walkersville, MD). Antibodies were purchased from BD Biosciences (mouse anti-Nck, mouse anti-GM130), Sigma (mouse anti-β actin), Invitrogen (mouse anti-GAPDH), Cell Signaling (mouse anti-phospho-myosin light chain2), Bender Med System (rabbit anti-VE-cadherin polyclonal), and Santa Cruz Biotechnology (goat anti-mouse IgG-HRP and goat anti-rabbit IgG-HRP). Other reagents were purchased from the following sources: DAPI (Sigma), fibronectin (Calbiochem/Invitrogen), recombinant human VEGF 165 (R&D systems), Matrigel® (BD Biosciences), Texas Red phalloidin (Invitrogen), Lipofectamine 2000 (Invitrogen), DMEM (HyClone), fetal bovine serum (BenchMark), Superscript III One-Step RT-PCR

System with Platinum Taq DNA polymerase (Invitrogen), RNeasy Plus kit (Qiagen), and Alexa Fluor 488 protein labeling kit (Invitrogen).

Cell culture

NIH 3T3 fibroblasts and Nck-deficient (deletion of Nck1 and Nck2) mouse embryonic fibroblasts were cultured in DMEM supplemented with antibiotics and 10% super calf serum. HEK293T cells were cultured in DMEM supplemented with antibiotics and 10% fetal bovine serum. HUVEC were cultured in dishes pre-coated with fibronectin (10 µg/ml) in endothelial cell EGM-2 complete medium with 2% fetal bovine serum, in an atmosphere of 5% CO_2/95% air. When required, cells were cultured in EBM-2 basal media supplemented with 0.2% fetal bovine serum as starvation media.

Plasmids and viral transduction

Viruses were generated in HEK293T cells transfected by calcium phosphate precipitation with p.Super.puro/YFP/Cherry carrying different oligonucleotide sequences (shRNA) targeting human Nck1 or Nck2 (protein knockdown). For protein expression, the pMSCV retroviral vector carrying a cDNA of mouse Nck2, human Nck2-YFP, human Nck-1, human β-actin-mCherry, or mouse paxillin-YFP was utilized. Each of these plasmids was cotransfected with pHCMV-G and pMD.gag.pol plasmids. Medium containing virus was harvested within 48 hours of transfection and stored at −80℃ in aliquots for later use. Target cells (HUVEC) were virally transduced essentially as described (Rivera et al., 2009). Two successive round of infection were done to increase the expression of shRNAs. The efficiency of transfection, judged by the expression of the fluorescent protein marker (YFP or mCherry), was consistently >90%. This strategy allowed population- and cell-based determinations without prior selection of a subpopulation of cells.

Western immunoblotting

Cells were harvested in ice-cold kinase lysis buffer (25 mM Tris, pH 7.4, 150 mM NaCl, 5 mM EDTA, 10% glycerol, 1% Triton X-100, 10 mM β-glycerophosphate, 1 mM sodium orthovanadate, 10 mM sodium pyrophosphate, 10 µg/ml aprotinin and 1 mM PMSF) and the supernatant was collected following high-speed cold centrifugation. For western immunoblotting, protein content from samples was determined by the Bradford Assay (Bio-Rad), and equal amounts of protein were subjected to SDS/PAGE. After transfer to nitrocellulose membranes and blocking in 0.5% nonfat dry milk, blots were probed with primary antibody followed, after several washes, by secondary antibody. Washed membranes were incubated in enhanced chemiluminescence substrate (NEL 100001EA, PerkinElmer Inc., Waltham, MA) for film exposure and development. All antibodies were diluted in 0.5% nonfat dry milk as 1:5000 for mouse anti-Nck (610099, BD Biosciences), 1:10000 for mouse anti-GAPDH (437000, Invitrogen), 1:2500 for mouse anti-β-Actin (A1978, Sigma) and 1:10000 for goat anti-mouse IgG-HRP (sc-2055, Santa Cruz Biotechnology). Images were analyzed using EMBL ImageJ software.

Imaging

Brightfield images and differential interference contrast (DIC) images were captured using an Olympus IX70 inverted microscope equipped with 10× and 20× dry DIC objectives. For membrane dynamics (kymography), a Zeiss Stallion microscope equipped with a Photometrics CoolSnap HQ or a Zeiss TIRF 3 microscope (Carl Zeiss Microimaging, Thornwood, NY) equiped with Photometrics Quant EM 512SC EMCCD camera was used. Time-lapse images were captured using a Plan-Apochromat 63×/1.40 oil DIC objective. Fluorescence images of fixed cells for gelatin matrix degradation and VE-cadherin cell–cell junction analysis were collected on a Zeiss LSM 510 Meta confocal microscope using a Plan-Neofluar 40×/1.3 oil objective. Time-lapse series of adhesion structures were captured by TIRF microscopy using the Zeiss TIRF 3 microscope equiped with a Plan-Apochromat 100×/1.46 oil objective lens. FRET imaging was performed on the Zeiss Stallion microscope configured with CFP-YFP FRET module.

AFM measurements

The integrated microscope system used for these studies combines AFM with TIRF and spinning-disk confocal microscopy (Trache and Lim, 2009). AFM experiments were performed with unsharpened silicon nitride cantilevers (MLCT, Bruker Nano-Surfaces Inc., Santa Barbara, CA) coated with fibronectin (FN, Invitrogen, 33016-015). After the cantilever is mounted on the glass holder, the tip is washed, and incubated for 5 minutes with 10 mg/ml polyethylene glycol used to cross-link FN onto tips at room temperature. The tip is then washed five times with deionized water, and subsequently incubated for 1 minute with 1 mg/ml FN. The tip is washed again five times with phosphate-buffered saline (Trache et al., 2005). The AFM was operated in force mode, by driving the cantilever to touch and retract from the cell surface over a known predefined distance in the z-axis. The z-axis movement of the cantilever and the deflection signal from the cantilever were recorded in a force curve. All force curves were acquired at positions midway between the nucleus and the edge of the cell for 2–3 minutes and repeated for ten cells in two separate experiments, for a total of ~2000 individual force curves. The adhesion force was calculated by multiplying the change in deflection height associated with the unbinding event by the spring constant of the cantilever (k=12.2±0.4 pN/nm). The local cell stiffness at the point of contact was calculated as Young's modulus of elasticity, by fitting the approach curve between the initial point of cell contact and point of maximum probe displacement with Sneddon's modified Hertz model (Trache et al., 2005). Kernel density plots of the distribution of force or elasticity measurements were generated using normal reference bandwidths and Gaussian kernel functions (Silverman, 1986) in NForceR software (Trzeciakowski and Meininger, NForceR: nanoscale force reader and AFM data analysis package, copyright 2004). These density plots were then analyzed using PeakFit (version 4.11, Systat Software Inc.) to provide accurate estimates of the peak value and associated confidence intervals for each distribution. For comparisons, peaks whose confidence intervals did not overlap were considered significantly different (P<0.05) (Venables and Ripley, 1997).

Analysis of membrane dynamics by kymography

Sub-confluent HUVEC plated on fibronectin (10 µg/ml)-coated 35 mm glass bottom MatTek dishes (MatTek corporation, Ashland, MA) were serum starved for 2 hours to monitor cellular responses to VEGF stimulation (50 ng/ml). Alternatively, cells were treated with a sodium azide solution (PBS supplemented with 0.1 g/l $CaCl_2$, 0.1 g/l $MgCl_2$ and 20 mM NaN3) for 30 minutes to induce ATP-actin monomer depletion and assess cellular responses following glucose replenishment (Bear et al., 2002). Images were collected every 15 seconds for various intervals as indicated for each particular experiment. For image analysis, one pixel line was drawn along the cell membrane and kymographs were generated using EMBL ImageJ. Quantitative parameters derived from kymographs were calculated as previously described (Hinz et al., 1999). Briefly, inspection of time-lapse series allowed the identification of protruding areas. Subsequently a one pixel-wide line crossing the edge of the cell perpendicularly at the location of the protrusion was traced. This lines records protrusion dynamics relative to the substratum since the position of the region of interest (the line) was fixed. Next, the snapshots corresponding to the line were lined up according to the sequence of image acquisition. The resulting images were displayed in a computer screen and shades of gray were used to identify protruding and retracting segments by manually drawing ascending and descending lines with a computer mouse using ImageJ segmented line tool. Dynamic data were generated from these segmented lines using 'read velocity tsp macro' of ImageJ. Raw data were transferred to an Excel spread sheet to calculate protrusion/retraction persistence and velocity, and ruffling frequency.

Analysis of focal adhesion dynamics

HUVECs expressing EYFP-paxillin were seeded at a density of 10×10^4 cells in 35-mm MatTek dishes 24 hours before imaging. Following exposure to sodium azide as detailed above, cells were washed and glucose-containing medium was replaced. Time lapse TIRF images were collected every 15 seconds for 30 minutes to 1 hour. Global assessment of focal adhesion dynamics was performed using a recently developed analysis system for the automated detection, tracking, and quantification of adhesion structures in living cells (Berginski et al., 2011). This is a unique tool that allows the assessment of adhesion dynamics in a comprehensive, unbiased manner. A total of 10–12 cells per experimental condition were analyzed. Spatially restricted analysis, i.e. dynamics of newly formed adhesions in protruding areas was determined by kymography as previously described (Webb et al., 2004). A total of 8–10 cells per experimental condition and 2–4 kymographs per cell were analyzed. A three pixel-wide line was drawn on the protruding areas to generate kymographs from fluorescence images using the software ImageJ. Following background subtraction, mean pixel density of the entire kymograph and longevity of individual adhesions were calculated. The elongation index was determined by ratio of the maximal long and perpendicular axes adhesions (Webb et al., 2004).

Analysis of Rho GTPase activation by FRET

The Raichu-Cdc42, Raichu-Rac1 and Raichu-RhoA intramolecular FRET biosensor used in this study has been described previously (Aoki and Matsuda, 2009). Raichu-Cdc42/Rac1/RhoA consist of truncated Cdc42/Rac1/RhoA and the Cdc42/Rac1/RhoA-interactive binding (CRIB) domain, sandwiched between a pair of green fluorescent protein (GFP) mutants, yellow fluorescent protein (YFP) and cyan fluorescent protein (CFP). In the inactive GDP-bound form, CFP and YFP remains apart from each other and excitation of CFP causes emission from CFP only. Activation caused by GTP loading bound form causes binding with CRIB domain and results in <10 nanometer-scale proximity of CFP and YFP. Consequently, excitation of CFP causes emission through YFP, hence FRET signal. Therefore, the FRET/CFP ratio is conveniently used as a representation of relative FRET efficiency. HUVEC plated on glass bottom MatTek dishes were transfected with plasmid containing Cdc42, Rac1, or RhoA FRET probes using lipofectamine 2000 (Invitrogen). After 24 hours of transfection, cells were washed and starved for 30 minutes. Following addition of 50 ng/ml VEGF and 10 mM HEPES in starvation medium, time-lapse images (CFP, FRET and YFP) were taken every 1 minute for 1 hour using a Zeiss Stallion microscope equipped with

the FRET module using a 63×/1.40 oil objective. Images were analyzed using EMBL ImageJ. Briefly, images were background corrected and a binary mask derived from the YFP image was multiplied separately by the background subtracted CFP and FRET images. Then FRET images were divided by CFP images to obtain FRET/CFP ratio images. A rainbow2 color LUT was applied and brightness and contrast were adjusted to display the ratio FRET images in an intensity modulated fashion where red indicates high and blue indicates low FRET efficiency, respectively. For quantitative analysis, background corrected and YFP masked FRET and CFP images were thresholded to measure pixel intensity of each individual image in the stack and FRET/CFP intensity ratios were calculated.

Analysis of cell polarity index

Confluent monolayers of HUVEC were grown on fibronectin-coated coverslips and serum starved for 6 hours. A horizontal wound was created in the confluent monolayer using a sterile 200 µl pipette tip. Following washing of cell debris with HBSS, HUVECs were incubated in EGM-2 complete medium with 2% fetal bovine serum at 37℃ in CO_2 incubator for 2 hours. Subsequently, cells were fixed in 3.7% paraformaldehyde in PBS for 10 minutes and permeabilized in 0.25% Triton X-100 in PBS for 5 minutes followed by 1 hour blocking in 2% BSA in PBS at room temperature. After blocking, cells were incubated for 1 hour in primary antibody (GM130; 1:100 in 2% BSA in PBS). Cells were subjected to an additional incubation of 1 hour with a mixture of a fluorescently-labeled secondary antibody, DAPI and TX Red phalloidin at room temperature. Cells were washed at least three times between each step. Following mounting, Images were captured using an Olympus IX70 microscope with 10× and 20× dry objectives. The polarity index was determined as previoulsy described (Etienne-Manneville and Hall, 2001). Briefly, cells in which the Golgi was located within the 120℃ angle facing the major axis of the wound were scored as polarized. A total of 120–150 cells from each of three independent experiments were analyzed to determine the polarity index.

Analysis of actin area

Actin area was measured from projections of confocal images. Cell and actin area were determined using the masking tool and image statistics tools available in the SlideBook software (Intelligent Imaging Innovations, Denver, CO). For comparisons, the protein area was normalized to the total cell area (Lim et al., 2010).

Statistics

For each experiment two to three independent replicates were conducted. Statistical comparisons among multiple groups were carried out by analysis of variance (ANOVA) followed by suitable post HOC tests (e.g. Tukey's test) using Minitab 16. Data presented in bar diagrams correspond to mean ± s.d. For data are presented in box and whiskers diagrams, the bold central lines of box plots indicate the median values whereas the top and bottom lines indicate the 3rd and 1st quartiles respectively. The whiskers extend up to 1.5 times the interquartile range.

Acknowledgements

We thank Professor Michiyuki Matsuda (Kyoto University) for the kind gift of the FRET Raichu probes and Dr Bruce Mayer (University of Connecticut Health Center) for graciously providing the paxillin-YFP construct. We thank Dr Robert Burghardt, Director of the Image Analysis Laboratory (TAMU College of Veterinary Medicine and Biomedical Sciences) for facilitating access to the imaging instrumentation and the critical reading of this manuscript. The excellent technical contribution of Mrs MacKenzie Limesand, Ms Rajeshwari Yog, Ms Kristine Bray, and Ms Deepika Ram is acknowledged. We thank Mr John Roths for his valuable help with image analysis and Dr Jerome Trzeciakowski (Texas A&M University Health Science Center) for advice on statistical analysis of atomic force microscopy data. This work is dedicated to the memory of our colleague Dr Don Hong.

Author contributions

S.P.C. and G.M.R. conceived and designed the experiments. S.P.C., R.B. and H.S. performed experiments. S.P.C., M.E.B., R.B., H.S., A.T., S.M.G. and G.M.R. analyzed the data. S.P.C., G.M.R., M.E.B. and S.M.G. contributed reagents, materials and/or analysis tools. S.P.C. and G.M.R. wrote the paper.

Funding

This work was supported by a Scientist Development Grant from the American Heart Association (AHA) [award number 0735282N] and start-up funds from Texas A&M University to G.M.R. H.S. was supported by a National Science Foundation (NSF) CAREER award [grant number 0747334 to A.T.].

Supplementary material available online at
http://jcs.biologists.org/lookup/suppl/doi:10.1242/jcs.119610/-/DC1

References

Abella, J. V., Vaillancourt, R., Frigault, M. M., Ponzo, M. G., Zuo, D., Sangwan, V., Larose, L. and Park, M. (2010). The Gab1 scaffold regulates RTK-dependent dorsal ruffle formation through the adaptor Nck. *J. Cell Sci.* **123**, 1306-1319.

Adams, R. H. and Alitalo, K. (2007). Molecular regulation of angiogenesis and lymphangiogenesis. *Nat. Rev. Mol. Cell Biol.* **8**, 464-478.

Antoku, S., Saksela, K., Rivera, G. M. and Mayer, B. J. (2008). A crucial role in cell spreading for the interaction of Abl PxxP motifs with Crk and Nck adaptors. *J. Cell Sci.* **121**, 3071-3082.

Aoki, K. and Matsuda, M. (2009). Visualization of small GTPase activity with fluorescence resonance energy transfer-based biosensors. *Nat. Protoc.* **4**, 1623-1631.

Barda-Saad, M., Braiman, A., Titerence, R., Bunnell, S. C., Barr, V. A. and Samelson, L. E. (2005). Dynamic molecular interactions linking the T cell antigen receptor to the actin cytoskeleton. *Nat. Immunol.* **6**, 80-89.

Bear, J. E., Svitkina, T. M., Krause, M., Schafer, D. A., Loureiro, J. J., Strasser, G. A., Maly, I. V., Chaga, O. Y., Cooper, J. A., Borisy, G. G. et al. (2002). Antagonism between Ena/VASP proteins and actin filament capping regulates fibroblast motility. *Cell* **109**, 509-521.

Berginski, M. E., Vitriol, E. A., Hahn, K. M. and Gomez, S. M. (2011). High-resolution quantification of focal adhesion spatiotemporal dynamics in living cells. *PLoS ONE* **6**, e22025.

Bladt, F., Aippersbach, E., Gelkop, S., Strasser, G. A., Nash, P., Tafuri, A., Gertler, F. B. and Pawson, T. (2003). The murine Nck SH2/SH3 adaptors are important for the development of mesoderm-derived embryonic structures and for regulating the cellular actin network. *Mol. Cell. Biol.* **23**, 4586-4597.

Bokoch, G. M. (2003). Biology of the p21-activated kinases. *Annu. Rev. Biochem.* **72**, 743-781.

Brown, M. C., Cary, L. A., Jamieson, J. S., Cooper, J. A. and Turner, C. E. (2005). Src and FAK kinases cooperate to phosphorylate paxillin kinase linker, stimulate its focal adhesion localization, and regulate cell spreading and protrusiveness. *Mol. Biol. Cell* **16**, 4316-4328.

Buday, L., Wunderlich, L. and Tamás, P. (2002). The Nck family of adapter proteins: regulators of actin cytoskeleton. *Cell. Signal.* **14**, 723-731.

Campellone, K. G., Rankin, S., Pawson, T., Kirschner, M. W., Tipper, D. J. and Leong, J. M. (2004). Clustering of Nck by a 12-residue Tir phosphopeptide is sufficient to trigger localized actin assembly. *J. Cell Biol.* **164**, 407-416.

Casaletto, J. B. and McClatchey, A. I. (2012). Spatial regulation of receptor tyrosine kinases in development and cancer. *Nat. Rev. Cancer* **12**, 387-400.

Choi, C. K., Vicente-Manzanares, M., Zareno, J., Whitmore, L. A., Mogilner, A. and Horwitz, A. R. (2008). Actin and alpha-actinin orchestrate the assembly and maturation of nascent adhesions in a myosin II motor-independent manner. *Nat. Cell Biol.* **10**, 1039-1050.

Dart, A. E., Donnelly, S. K., Holden, D. W., Way, M. and Caron, E. (2012). Nck and Cdc42 co-operate to recruit N-WASP to promote FcγR-mediated phagocytosis. *J. Cell Sci.* **125**, 2825-2830.

Delorme-Walker, V. D., Peterson, J. R., Chernoff, J., Waterman, C. M., Danuser, G., DerMardirossian, C. and Bokoch, G. M. (2011). Pak1 regulates focal adhesion strength, myosin IIA distribution, and actin dynamics to optimize cell migration. *J. Cell Biol.* **193**, 1289-1303.

Ditlev, J. A., Michalski, P. J., Huber, G., Rivera, G. M., Mohler, W. A., Loew, L. M. and Mayer, B. J. (2012). Stoichiometry of Nck-dependent actin polymerization in living cells. *J. Cell Biol.* **197**, 643-658.

Dodding, M. P. and Way, M. (2009). Nck- and N-WASP-dependent actin-based motility is conserved in divergent vertebrate poxviruses. *Cell Host Microbe* **6**, 536-550.

Eden, S., Rohatgi, R., Podtelejnikov, A. V., Mann, M. and Kirschner, M. W. (2002). Mechanism of regulation of WAVE1-induced actin nucleation by Rac1 and Nck. *Nature* **418**, 790-793.

Etienne-Manneville, S. and Hall, A. (2001). Integrin-mediated activation of Cdc42 controls cell polarity in migrating astrocytes through PKCzeta. *Cell* **106**, 489-498.

Etienne-Manneville, S. and Hall, A. (2002). Rho GTPases in cell biology. *Nature* **420**, 629-635.

Friedl, P. and Wolf, K. (2010). Plasticity of cell migration: a multiscale tuning model. *J. Cell Biol.* **188**, 11-19.

Funasaka, K., Ito, S., Hasegawa, H., Goldberg, G. S., Hirooka, Y., Goto, H., Hamaguchi, M. and Senga, T. (2010). Cas utilizes Nck2 to activate Cdc42 and regulate cell polarization during cell migration in response to wound healing. *FEBS J.* **277**, 3502-3513.

Galisteo, M. L., Chernoff, J., Su, Y. C., Skolnik, E. Y. and Schlessinger, J. (1996). The adaptor protein Nck links receptor tyrosine kinases with the serine-threonine kinase Pak1. *J. Biol. Chem.* **271**, 20997-21000.

Gardel, M. L., Schneider, I. C., Aratyn-Schaus, Y. and Waterman, C. M. (2010). Mechanical integration of actin and adhesion dynamics in cell migration. *Annu. Rev. Cell Dev. Biol.* **26**, 315-333.

Geiger, B. and Yamada, K. M. (2011). Molecular architecture and function of matrix adhesions. *Cold Spring Harb. Perspect. Biol.* **3**, 3.
Gruenheid, S., DeVinney, R., Bladt, F., Goosney, D., Gelkop, S., Gish, G. D., Pawson, T. and Finlay, B. B. (2001). Enteropathogenic E. coli Tir binds Nck to initiate actin pedestal formation in host cells. *Nat. Cell Biol.* **3**, 856-859.
Guan, S., Chen, M., Woodley, D. and Li, W. (2007). Nckbeta adapter controls neuritogenesis by maintaining the cellular paxillin level. *Mol. Cell. Biol.* **27**, 6001-6011.
Guan, S., Fan, J., Han, A., Chen, M., Woodley, D. T. and Li, W. (2009). Non-compensating roles between Nckalpha and Nckbeta in PDGF-BB signaling to promote human dermal fibroblast migration. *J. Invest. Dermatol.* **129**, 1909-1920.
Hinz, B., Alt, W., Johnen, C., Herzog, V. and Kaiser, H. W. (1999). Quantifying lamella dynamics of cultured cells by SACED, a new computer-assisted motion analysis. *Exp. Cell Res.* **251**, 234-243.
Hu, T., Shi, G., Larose, L., Rivera, G. M., Mayer, B. J. and Zhou, R. (2009). Regulation of process retraction and cell migration by EphA3 is mediated by the adaptor protein Nck1. *Biochemistry* **48**, 6369-6378.
Humphries, J. D., Byron, A. and Humphries, M. J. (2006). Integrin ligands at a glance. *J. Cell Sci.* **119**, 3901-3903.
Huttenlocher, A. and Horwitz, A. R. (2011). Integrins in cell migration. *Cold Spring Harb. Perspect. Biol.* **3**, a005074.
Jones, N., Blasutig, I. M., Eremina, V., Ruston, J. M., Bladt, F., Li, H., Huang, H., Larose, L., Li, S. S., Takano, T. et al. (2006). Nck adaptor proteins link nephrin to the actin cytoskeleton of kidney podocytes. *Nature* **440**, 818-823.
Kuo, J. C., Han, X., Hsiao, C. T., Yates, J. R., 3rd and Waterman, C. M. (2011). Analysis of the myosin-II-responsive focal adhesion proteome reveals a role for β-Pix in negative regulation of focal adhesion maturation. *Nat. Cell Biol.* **13**, 383-393.
Lamalice, L., Houle, F. and Huot, J. (2006). Phosphorylation of Tyr1214 within VEGFR-2 triggers the recruitment of Nck and activation of Fyn leading to SAPK2/p38 activation and endothelial cell migration in response to VEGF. *J. Biol. Chem.* **281**, 34009-34020.
Lapetina, S., Mader, C. C., Machida, K., Mayer, B. J. and Koleske, A. J. (2009). Arg interacts with cortactin to promote adhesion-dependent cell edge protrusion. *J. Cell Biol.* **185**, 503-519.
Lauffenburger, D. A. and Horwitz, A. F. (1996). Cell migration: a physically integrated molecular process. *Cell* **84**, 359-369.
Lebensohn, A. M. and Kirschner, M. W. (2009). Activation of the WAVE complex by coincident signals controls actin assembly. *Mol. Cell* **36**, 512-524.
Lettau, M., Qian, J., Linkermann, A., Latreille, M., Larose, L., Kabelitz, D. and Janssen, O. (2006). The adaptor protein Nck interacts with Fas ligand: Guiding the death factor to the cytotoxic immunological synapse. *Proc. Natl. Acad. Sci. USA* **103**, 5911-5916.
Lettau, M., Pieper, J. and Janssen, O. (2009). Nck adapter proteins: functional versatility in T cells. *Cell Commun. Signal.* **7**, 1.
Li, W., Fan, J. and Woodley, D. T. (2001). Nck/Dock: an adapter between cell surface receptors and the actin cytoskeleton. *Oncogene* **20**, 6403-6417.
Lim, S. M., Kreipe, B. A., Trzeciakowski, J., Dangott, L. and Trache, A. (2010). Extracellular matrix effect on RhoA signaling modulation in vascular smooth muscle cells. *Exp. Cell Res.* **316**, 2833-2848.
Lim, S. M., Trzeciakowski, J. P., Sreenivasappa, H., Dangott, L. J. and Trache, A. (2012). RhoA-induced cytoskeletal tension controls adaptive cellular remodeling to mechanical signaling. *Integr Biol. (Camb)* **4**, 615-627.
Lu, W., Katz, S., Gupta, R. and Mayer, B. J. (1997). Activation of Pak by membrane localization mediated by an SH3 domain from the adaptor protein Nck. *Curr. Biol.* **7**, 85-94.
Machacek, M., Hodgson, L., Welch, C., Elliott, H., Pertz, O., Nalbant, P., Abell, A., Johnson, G. L., Hahn, K. M. and Danuser, G. (2009). Coordination of Rho GTPase activities during cell protrusion. *Nature* **461**, 99-103.
Machida, K. and Mayer, B. J. (2005). The SH2 domain: versatile signaling module and pharmaceutical target. *Biochim. Biophys. Acta* **1747**, 1-25.
Moreau, V., Frischknecht, F., Reckmann, I., Vincentelli, R., Rabut, G., Stewart, D. and Way, M. (2000). A complex of N-WASP and WIP integrates signalling cascades that lead to actin polymerization. *Nat. Cell Biol.* **2**, 441-448.
Nelson, W. J. (2009). Remodeling epithelial cell organization: transitions between front-rear and apical-basal polarity. *Cold Spring Harb. Perspect. Biol.* **1**, a000513.
Oser, M., Yamaguchi, H., Mader, C. C., Bravo-Cordero, J. J., Arias, M., Chen, X., Desmarais, V., van Rheenen, J., Koleske, A. J. and Condeelis, J. (2009). Cortactin regulates cofilin and N-WASp activities to control the stages of invadopodium assembly and maturation. *J. Cell Biol.* **186**, 571-587.
Oser, M., Mader, C. C., Gil-Henn, H., Magalhaes, M., Bravo-Cordero, J. J., Koleske, A. J. and Condeelis, J. (2010). Specific tyrosine phosphorylation sites on cortactin regulate Nck1-dependent actin polymerization in invadopodia. *J. Cell Sci.* **123**, 3662-3673.
Paik, J. H., Chae, S. s., Lee, M. J., Thangada, S. and Hla, T. (2001). Sphingosine 1-phosphate-induced endothelial cell migration requires the expression of EDG-1 and EDG-3 receptors and Rho-dependent activation of alpha vbeta3- and beta1-containing integrins. *J. Biol. Chem.* **276**, 11830-11837.
Parrini, M. C., Sadou-Dubourgnoux, A., Aoki, K., Kunida, K., Biondini, M., Hatzoglou, A., Poullet, P., Formstecher, E., Yeaman, C., Matsuda, M. et al. (2011). SH3BP1, an exocyst-associated RhoGAP, inactivates Rac1 at the front to drive cell motility. *Mol. Cell* **42**, 650-661.
Pawson, T. (2004). Specificity in signal transduction: from phosphotyrosine-SH2 domain interactions to complex cellular systems. *Cell* **116**, 191-203.
Petrie, R. J., Doyle, A. D. and Yamada, K. M. (2009). Random versus directionally persistent cell migration. *Nat. Rev. Mol. Cell Biol.* **10**, 538-549.
Pils, S., Kopp, K., Peterson, L., Delgado Tascón, J., Nyffenegger-Jann, N. J. and Hauck, C. R. (2012). The adaptor molecule Nck localizes the WAVE complex to promote actin polymerization during CEACAM3-mediated phagocytosis of bacteria. *PLoS ONE* **7**, e32808.
Ridley, A. J. (2012). Historical overview of Rho GTPases. *Methods Mol. Biol.* **827**, 3-12.
Rivera, G. M., Briceño, C. A., Takeshima, F., Snapper, S. B. and Mayer, B. J. (2004). Inducible clustering of membrane-targeted SH3 domains of the adaptor protein Nck triggers localized actin polymerization. *Curr. Biol.* **14**, 11-22.
Rivera, G. M., Antoku, S., Gelkop, S., Shin, N. Y., Hanks, S. K., Pawson, T. and Mayer, B. J. (2006). Requirement of Nck adaptors for actin dynamics and cell migration stimulated by platelet-derived growth factor B. *Proc. Natl. Acad. Sci. USA* **103**, 9536-9541.
Rivera, G. M., Vasilescu, D., Papayannopoulos, V., Lim, W. A. and Mayer, B. J. (2009). A reciprocal interdependence between Nck and PI(4,5)P(2) promotes localized N-WASp-mediated actin polymerization in living cells. *Mol. Cell* **36**, 525-535.
Rodriguez, L. G., Wu, X. and Guan, J. L. (2004). Wound-healing assay. *Methods Mol. Biol.* **294**, 23-29.
Ruusala, A., Pawson, T., Heldin, C. H. and Aspenström, P. (2008). Nck adapters are involved in the formation of dorsal ruffles, cell migration, and Rho signaling downstream of the platelet-derived growth factor beta receptor. *J. Biol. Chem.* **283**, 30034-30044.
Scaplehorn, N., Holmström, A., Moreau, V., Frischknecht, F., Reckmann, I. and Way, M. (2002). Grb2 and Nck act cooperatively to promote actin-based motility of vaccinia virus. *Curr. Biol.* **12**, 740-745.
Silverman, B. W. (1986). *Density Estimation for Statistics and Data Analysis (Monographs on Statistics and Applied Probability)*. London: Chapman & Hall.
Stoletov, K. V., Ratcliffe, K. E., Spring, S. C. and Terman, B. I. (2001). NCK and PAK participate in the signaling pathway by which vascular endothelial growth factor stimulates the assembly of focal adhesions. *J. Biol. Chem.* **276**, 22748-22755.
Stoletov, K. V., Gong, C. and Terman, B. I. (2004). Nck and Crk mediate distinct VEGF-induced signaling pathways that serve overlapping functions in focal adhesion turnover and integrin activation. *Exp. Cell Res.* **295**, 258-268.
Stylli, S. S., Stacey, T. T., Verhagen, A. M., Xu, S. S., Pass, I., Courtneidge, S. A. and Lock, P. (2009). Nck adaptor proteins link Tks5 to invadopodia actin regulation and ECM degradation. *J. Cell Sci.* **122**, 2727-2740.
Suetsugu, S., Yamazaki, D., Kurisu, S. and Takenawa, T. (2003). Differential roles of WAVE1 and WAVE2 in dorsal and peripheral ruffle formation for fibroblast cell migration. *Dev. Cell* **5**, 595-609.
Svitkina, T. M., Neyfakh, A. A., Jr and Bershadsky, A. D. (1986). Actin cytoskeleton of spread fibroblasts appears to assemble at the cell edges. *J. Cell Sci.* **82**, 235-248.
Trache, A. and Lim, S. M. (2009). Integrated microscopy for real-time imaging of mechanotransduction studies in live cells. *J. Biomed. Opt.* **14**, 034024.
Trache, A., Trzeciakowski, J. P., Gardiner, L., Sun, Z., Muthuchamy, M., Guo, M., Yuan, S. Y. and Meininger, G. A. (2005). Histamine effects on endothelial cell fibronectin interaction studied by atomic force microscopy. *Biophys. J.* **89**, 2888-2898.
Uetrecht, A. C. and Bear, J. E. (2009). Golgi polarity does not correlate with speed or persistence of freely migrating fibroblasts. *Eur. J. Cell Biol.* **88**, 711-717.
Vaynberg, J., Fukuda, T., Chen, K., Vinogradova, O., Velyvis, A., Tu, Y., Ng, L., Wu, C. and Qin, J. (2005). Structure of an ultraweak protein-protein complex and its crucial role in regulation of cell morphology and motility. *Mol. Cell* **17**, 513-523.
Venables, W. and Ripley, B. (1997). Modern Applied Statistics with S-PLUS. New York: Springer.
Verma, R., Kovari, I., Soofi, A., Nihalani, D., Patrie, K. and Holzman, L. B. (2006). Nephrin ectodomain engagement results in Src kinase activation, nephrin phosphorylation, Nck recruitment, and actin polymerization. *J. Clin. Invest.* **116**, 1346-1359.
Vicente-Manzanares, M., Zareno, J., Whitmore, L., Choi, C. K. and Horwitz, A. F. (2007). Regulation of protrusion, adhesion dynamics, and polarity by myosins IIA and IIB in migrating cells. *J. Cell Biol.* **176**, 573-580.
Vicente-Manzanares, M., Ma, X., Adelstein, R. S. and Horwitz, A. R. (2009). Non-muscle myosin II takes centre stage in cell adhesion and migration. *Nat. Rev. Mol. Cell Biol.* **10**, 778-790.
Vicente-Manzanares, M., Newell-Litwa, K., Bachir, A. I., Whitmore, L. A. and Horwitz, A. R. (2011). Myosin IIA/IIB restrict adhesive and protrusive signaling to generate front-back polarity in migrating cells. *J. Cell Biol.* **193**, 381-396.
Webb, D. J., Donais, K., Whitmore, L. A., Thomas, S. M., Turner, C. E., Parsons, J. T. and Horwitz, A. F. (2004). FAK-Src signalling through paxillin, ERK and MLCK regulates adhesion disassembly. *Nat. Cell Biol.* **6**, 154-161.
Wu, C., Asokan, S. B., Berginski, M. E., Haynes, E. M., Sharpless, N. E., Griffith, J. D., Gomez, S. M. and Bear, J. E. (2012). Arp2/3 is critical for lamellipodia and response to extracellular matrix cues but is dispensable for chemotaxis. *Cell* **148**, 973-987.
Zinchuk, V. and Zinchuk, O. (2008). Quantitative colocalization analysis of confocal fluorescence microscopy images. *Curr. Protoc Cell Biol.* **Suppl. 39**, 4.19.1-4.19.16.

Journal of Cell Science